Atomic Collapse and Quasi–Rydberg States in Graphene

A. V. Shytov,[1] M. I. Katsnelson,[2] and L. S. Levitov[3]

[1]*Brookhaven National Laboratory, Upton, New York 11973-5000, USA*

[2]*Radboud University of Nijmegen, Toernooiveld 1 6525 ED Nijmegen, The Netherlands*

[3]*Department of Physics, Massachusetts Institute of Technology, 77 Massachusetts Ave, Cambridge, Massachusetts 02139, USA*

(Received 6 August 2007; published 14 December 2007)

Charge impurities in graphene can host an infinite family of Rydberg-like resonance states of massless Dirac particles. These states, appearing for supercritical charge, are described by Bohr-Sommerfeld quantization of *collapsing* classical trajectories that descend on point charge, in analogy to the hydrogenic Rydberg states relation with planetary orbits. Strong tunnel coupling of these states to the Dirac continuum leads to resonance features in scattering on the impurities that manifest themselves in transport properties and in the local density of states.

DOI: 10.1103/PhysRevLett.99.246802 PACS numbers: 81.05.Uw

The discovery of massless Dirac excitations in graphene [1] triggered interest in solid-state realization of quantum electrodynamics (QED) [2–4]. Transport in this system can be used to probe the fundamental concepts of QED such as chiral dynamics [3,5], the flavor degrees of freedom [6], and particle-hole coexistence [7]. Here, we demonstrate that graphene opens a way to investigate in the laboratory a fundamental quantum relativistic phenomenon, that is, atomic collapse in a strong Coulomb electric field [8,9]. Predicted a long time ago, it remained elusive in the high-energy experiments [10].

Bohr's theory explained that stability of an atom results from the quantum mechanical zero-point motion that prevents electron from falling on a nucleus. This balance becomes more delicate in the relativistic theory. The effects undermining the stability of matter arise already in classical dynamics, where electron trajectory can spiral around the nucleus and eventually fall on it [11] [see Fig. 1(a) and 1(b)]. The collapse occurs whenever the electron angular momentum is small enough: $M < M_c = Ze^2/c$, where Z is the number of protons in the nucleus. Quantum mechanics saves atoms from imploding by imposing the quantization condition $M = n\hbar$. This stabilizes all sufficiently light atoms with $Z < \hbar c/e^2 \approx 137$.

Early work on the Dirac-Kepler problem has revealed bizarre properties of atoms with nuclear charge in excess of 137 that pose a fundamental bound on the periodic table of elements extent to large Z. The breakdown at $Z > 137$ of the low-Z solution of the Dirac equation arises because the Dirac operator with supercritical Coulomb potential is not self-adjoint. This problem can be fixed by accounting for a finite nuclear radius [12]. The resulting electron states dive into the hole continuum at $Z > 170$ and decay by positron emission [8,9]. These phenomena, never observed in the laboratory due to the difficulty of producing heavy nuclei, should be more readily accessible in graphene owing to its large "fine structure constant," $\alpha = e^2/\hbar v_F \approx 2.5$, where $v_F \approx 10^6$ m/s is the velocity of Dirac excitations.

Charge impurities are an essential ingredient of our current understanding of transport in graphene. Scattering on charge impurities explains [13–15] the linear density dependence of conductivity in this material [16], and is thus regarded as one of the main factors limiting carrier mobility. Recent investigations of screening of impurity potential [17–21] have only reinforced these conclusions, making graphene an ideal test system for the theory of Coulomb scattering [18,22] of massless Dirac particles.

In this Letter, we show that, although massless particles cannot form bound states, an infinite family of quasibound states appears abruptly when the Coulomb potential strength exceeds a certain critical value $\beta = \frac{1}{2}$. These states are obtained from Bohr-Sommerfeld quantization of *collapsing orbits* which descend on the point charge, similar to how the hydrogenic Rydberg states are found from circular orbits. The energies of these states converge

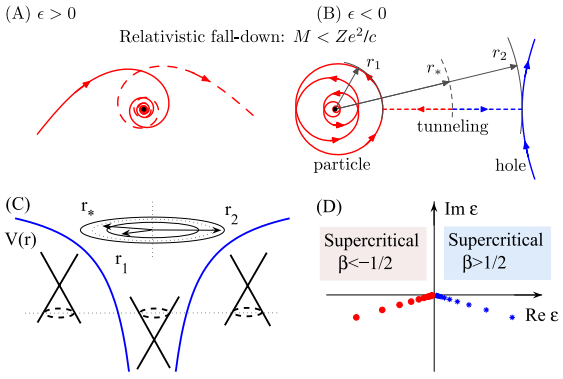

FIG. 1 (color online). Classical and quantum picture of atomic collapse due to electron with angular momentum $M < M_c$ falling on the nucleus. Trajectories obtained from (1) for (a) positive and (b) negative energy ε of a massless Dirac particle are shown. At $\varepsilon < 0$, there are collapsing particle trajectories and noncollapsing hole trajectories (b,c), separated by a classically forbidden region, the annulus $r_1 < r < r_2$ ($r_{1,2} = r_* \mp Mv_F/\varepsilon$, $r_* = Ze^2/|\varepsilon|$). Tunnel coupling to the continuum at $r > r_2$ defines a family of quasistationary states with complex energy spectrum (d), appearing abruptly when the potential strength exceeds the stability threshold $|\beta| = \frac{1}{2}$.

on zero, $\varepsilon_n \to 0$ at large n, whereas their radii diverge, similar to the Rydberg states. These results are corroborated by an exact solution of the 2D Dirac-Kepler problem. In graphene, the effective Coulomb potential strength [18] is given by $\beta = Ze^2/\kappa\hbar v_F$ with intrinsic dielectric constant $\kappa \approx 5$, and therefore the critical value $\beta = \frac{1}{2}$ can be reached already for the impurity charge $Z \gtrsim 1$. This is a lot more convenient from the experimental point of view than $Z > 170$ in heavy atoms.

The quasi–Rydberg states hybridize with the Dirac continuum via the Klein tunneling process that couples particles and antiparticles [9]. This hybridization leads to strong resonances in the scattering cross-section, manifest in transport, and to striking effects in local properties that can be probed by introducing impurities with $Z \gtrsim 1$ in graphene. Univalent charge impurities, such as K, Na, or NH_3, all commonly used in graphene, are on the border of the supercritical regime. To investigate this regime experimentally, one can use divalent or trivalent dopants such as alkaline-earth or rare-earth metals. They are frequently used to prepare intercalated graphite compounds [23], e.g., Ca and Yb [24] ($Z = 2$), La [25] and Gd [26] ($Z = 3$). Recently, spectroscopic experiments on graphene doped by Ca have been reported [27].

Recent literature [17–21] investigated screening of charge impurities by polarization of the Dirac vacuum [18]. The effects of vacuum polarization are inconsequential in atomic physics due to its short spatial scale set by the Compton wavelength $\lambda = h/mc \approx 2.4 \times 10^{-3}$ nm. In the massless case of graphene, however, it leads to a long-range polarization appearing above the critical value $\beta = \frac{1}{2}$ of the impurity charge [18]. These studies indicate that $\beta = \frac{1}{2}$ separates two very different regimes of screening, essentially perturbative at $\beta < \frac{1}{2}$ [17,20], and nonlinear at $\beta > \frac{1}{2}$ [18,19,21].

To explain why the quasibound states appear at large β, we consider fermions with energy $\varepsilon < 0$ in the potential $V(r) = -Ze^2/r$. Since the kinetic energy $K = \varepsilon - V(r)$ vanishes at $r_* = Ze^2/|\varepsilon|$, the polarity of carriers changes sign inside the disk $r < r_*$ [see Fig. 1(c)]. If r_* exceeds particle wavelength $\lambda = \hbar v_F/|\varepsilon|$, which happens for $\beta = Ze^2/\hbar v_F \gtrsim 1$, quantum states can be trapped at $r \lesssim r_*$. These states will have finite lifetime due to Klein tunneling through the barrier at $r \approx r_*$. Crucially, since the ratio r_*/λ is independent of ε, this reasoning predicts infinitely many quasibound states [see Fig. 1(d)].

We obtain these states quasiclassically from relativistic dynamics with $H = v_F|\mathbf{p}| - Ze^2/r$. The collapsing trajectories with angular momenta $M < M_c = Ze^2/v_F$ are separated from nonfalling trajectories by a centrifugal barrier. This is manifest in the radial dynamics

$$p_r^2 = v_F^{-2}\left(\varepsilon + \frac{Ze^2}{r}\right)^2 - \frac{M^2}{r^2}, \tag{1}$$

where p_r is the radial momentum. This defines a classically forbidden region, the annulus $r_1 < r < r_2$, $r_{1,2} = (Ze^2 \mp Mv_F)/\varepsilon$, where (1) is negative. The quasibound states trapped by this barrier can be found from the Bohr-Sommerfeld quantization condition $\int_{r_0}^{r_1} p_r dr = \pi\hbar n$, where r_0 is the lattice cutoff (cf. Refs. [28,29]). Evaluating the integral with logarithmic accuracy, we obtain $\gamma \ln\frac{Ze^2}{r_0\varepsilon} = \pi\hbar n$, where $\gamma \equiv (M_c^2 - M^2)^{1/2}$, which gives the quasi–Rydberg states

$$\varepsilon_n \approx \frac{Ze^2}{r_0} e^{-\pi\hbar n/\gamma}, \qquad n > 0. \tag{2}$$

The energies (2) are equally spaced on the log scale with the separation diverging as $1/\gamma$ at the threshold $M_c \approx M$.

To find the transparency of the barrier, we integrate $\mathrm{Im}\, p_r$ to obtain the tunneling action

$$S = \int_{r_1}^{r_2} dr \sqrt{\frac{M^2}{r^2} - \left(\frac{\varepsilon}{v_F} + \frac{M_c}{r}\right)^2} = \pi(M_c - \gamma). \tag{3}$$

Taken near the threshold $\gamma \approx 0$, the transparency $e^{-2S/\hbar}$ gives the width $\Gamma_n \sim |\varepsilon_n| \exp(-2\pi Ze^2/\hbar v_F)$. Notably, since S has no energy dependence, all the states (2) feature the same width-to-energy ratio.

It is instructive to compare these results to the exact solution of the Coulomb scattering problem. For that, we consider the Dirac equation for a massless electron in a potential $V(r) = \frac{\beta}{r}$, where $\beta \equiv -Ze^2/\hbar v_F$. (We include the minus sign in β to explicitly account for attraction.) After uneventful angular decomposition, solving the radial equation separately in each angular momentum channel [18], we find the scattering phases $\delta_m(k)$ that behave differently in the three regimes: (i) $\beta > |\beta_m|$, (ii) $-|\beta_m| < \beta < |\beta_m|$, and (iii) $\beta < -|\beta_m|$, where $\beta_m = m + \frac{1}{2}$ is the angular momentum. As illustrated in Fig. 2(a), $\delta_m(k)$ are energy-independent in case (ii) and have a logarithmic dependence $\delta_m(k) \sim -\gamma \ln kr_0$ in case (i), where $\gamma = \sqrt{\beta^2 - \beta_m^2}$. In the case (iii), the dependence is described by kinks of height π that signal the appearance of quasibound states:

$$e^{2i\delta_m(k)} = e^{\pi i|\beta_m|} \frac{z + e^{2i\chi(k)}}{1 + e^{2i\chi(k)}z^*}, \tag{4}$$

[see [18], Eq. (20)] where $z = \frac{e^{\pi\gamma}}{\eta} \frac{\Gamma(1+2i\gamma)}{\Gamma(1-2i\gamma)} \frac{\Gamma(1-i\gamma+i\beta)}{\Gamma(1+i\gamma+i\beta)}$, and

$$\chi(k) = \gamma \ln 2kr_0 + \arctan\frac{1+\eta}{1-\eta}, \qquad \eta = \sqrt{\frac{\beta-\gamma}{\beta+\gamma}}. \tag{5}$$

To find the quasibound states, we seek a scattering state with complex energy in which there is no incoming wave. This implies vanishing of the numerator (denominator) of (4) at $\varepsilon < 0$ ($\varepsilon > 0$). In the former case, we obtain an equation $e^{i\chi(k)} = -z$, where $|z| \neq 1$, and thus it is impossible to satisfy it by a real k. Complex solutions of $2\chi(k) = -i\ln(-z) - 2\pi n$ resemble the quasiclassical ones, Eq. (2). Near the threshold $\beta = |\beta_m|$, expanding in small γ, we find the complex solutions

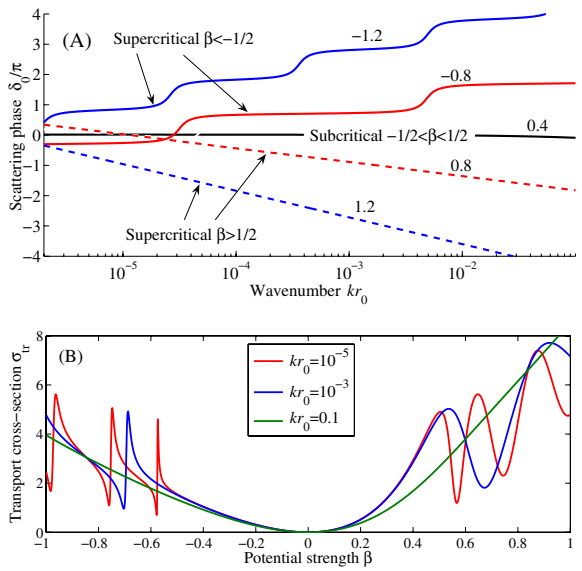

FIG. 2 (color online). (a) Scattering phase δ_0 at negative energy $\varepsilon = -v_F k < 0$. The kinks correspond to the quasibound states trapped by the impurity potential of supercritical strength $\beta < -1/2$, as illustrated in Fig. 1. (b) Transport cross-section (10) *vs.* potential strength. Fano resonances corresponding to quasibound states occur at $\beta < -\frac{1}{2}$. The oscillatory behavior at $\beta > \frac{1}{2}$ results from the energy dependence $\delta_m(k) \sim -\gamma_m \ln kr_0$. The cross section asymmetry upon $\beta \to -\beta$, with the values at $\beta < 0$ typically lower than at $\beta > 0$, reflects that incoming particles in Fig. 1(b) are prevented from reaching the region of strong scattering $r \sim 0$.

$$k_n = ce^{-(\pi/\gamma)n - i\lambda}, \qquad n > 0, \tag{6}$$

where $\lambda = \frac{\pi}{1-e^{-2\pi\beta}}$ and the prefactor c is of order r_0^{-1}. We have $\arg k_n \approx 0.045\pi$, such that k_n have small imaginary parts, defining sharp resonances of width

$$\frac{1}{2}\Gamma = -\mathrm{Im}\varepsilon = \frac{\pi}{e^{\pi}-1}|\varepsilon| \approx 0.14|\varepsilon|. \tag{7}$$

Before discussing manifestations in graphene, where the $1/r$ potential is screened, we note that screening will not affect the essential physics as long as the quasibound states persist. At finite doping, the RPA screening length exceeds the Fermi wavelength $\lambda_F = \hbar v_F/\varepsilon_F$ [13–15], whereas our quasiclassical estimate of the state radius gives $r_1 \approx (M_c - M)v_F/|\varepsilon| = (\beta - \frac{1}{2})\hbar v_F/|\varepsilon|$. The latter is much smaller than λ_F near $\beta = \frac{1}{2}$, which means that RPA screening is nondetrimental for the states with $\varepsilon_n \gtrsim \varepsilon_F$. At the same time, the states with $\varepsilon \lesssim \varepsilon_F$ are too shallow to form in the screened potential.

However, as discussed in [18], screening in the supercritical regime is dominated by the nonlinear effects that bring the effective charge down to the critical value. The characteristic radius of the screening cloud [18], at zero doping and not too strong interaction, $\alpha = e^2/\kappa\hbar v_F \lesssim 1$, is $\rho_* = r_0 \exp[\frac{\pi}{4\alpha}\cosh^{-1}(2\beta)]$. Only the states (6) having radius less than ρ_* will be unaffected by screening. Comparing ρ_* with our expression for r_1, we find that the threshold for the appearance of the resonances is shifted towards stronger potential values: $\beta_c = \frac{1}{2} + O(\alpha)$.

Resonance scattering on the quasibound states will manifest itself in the dependence of transport properties on the carrier density. Here, we analyze electrical conductivity described by the Drude-like model (see Ref. [13]):

$$\sigma = \frac{e^2}{h} 2\varepsilon_F \tau, \qquad \tau^{-1} = v_F n_{\mathrm{imp}} \sigma_{\mathrm{tr}}, \tag{8}$$

where ε_F is the Fermi energy, n_{imp} is the concentration of charge impurities, and σ_{tr} is the transport scattering cross-section for one impurity. We use the 2D scattering amplitude partial wave decomposition

$$f(\varphi) = \frac{2i}{\sqrt{2\pi ik}} \sum_{m=0}^{\infty} (e^{2i\delta_m} - 1)\cos\left(m + \frac{1}{2}\right)\varphi, \tag{9}$$

[see Ref. [4], Eq. (47)] to evaluate transport cross section

$$\sigma_{\mathrm{tr}} = \int d\varphi (1 - \cos\varphi)|f(\varphi)|^2 = \frac{4}{k}\sum_{m=0}^{\infty} \sin^2\theta_m, \tag{10}$$

$\theta_m = \delta_m - \delta_{m+1}$, with the phases δ_m given by (4) for overcritical channels (see Ref. [22] for subcritical channels).

For subcritical potential strength, the phases are energy-independent and thus σ_{tr} scales as $1/|\varepsilon|$, giving conductivity (8) linear in the carrier density [13–15]. For $|\beta| > \frac{1}{2}$, the contribution of the subcritical channels still scales as $1/|\varepsilon|$, while the overcritical channels, because of energy-dependent $\delta_m(k)$, give an oscillatory contribution. These oscillations, shown in Figs. 2(b) and 3 inset, have a characteristic form of Fano resonances resulting from kinks in the scattering phase at the energies ε_n. In this regime, the conductivity (8) exhibits peaks at the densities for which the Fermi level ε_F aligns with ε_n. As evident from Fig. 3, the peak position is highly sensitive to the potential strength β, changing by an order of magnitude when β varies from -1.0 to -1.3, which is a combined effect of ε_F quadratic dependence on density and of the exponential dependence in (6).

Another striking feature in the conductivity *vs.* density plots in Fig. 3 is the particle/hole asymmetry, which results from the scattering cross section being typically lower at $\varepsilon < 0$ than at $\varepsilon > 0$. Such asymmetry, noted already in the subcritical regime [22], becomes more prominent in the supercritical regime because of the Klein barrier preventing particles with negative energies from reaching the strong scattering region $r \sim 0$ [cf. Figure 1(b)].

The signatures of quasibound states, similar to those in conductivity, will be featured by other transport coefficients. In particular, they will be strong in the thermoelectric response because it is proportional to the energy derivative of σ_{tr}. Yet, the most direct way to observe these states is via the local density of states (LDOS)

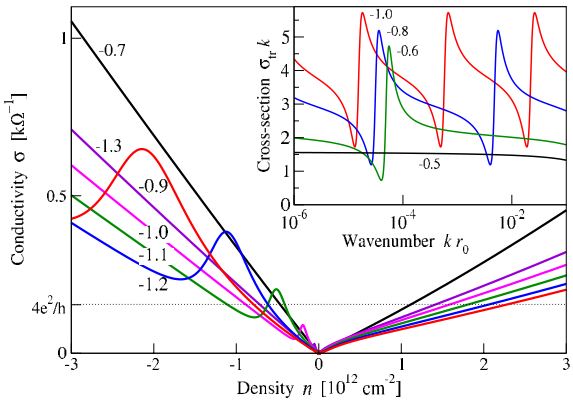

FIG. 3 (color online). Peak structure in the ohmic conductivity (8) and (10), for overcritical β occurring when the Fermi energy is aligned with resonances. The values of β are indicated near each trace. (Parameters used: $n_{\mathrm{imp}} = 3 \times 10^{11}$ cm^{-2}, $r_0 = 0.25$ nm) Inset: Fano resonance structure in the cross section (10) at negative energies with the overall $1/k$ dependence factored out.

$$\nu(\varepsilon, r) = \frac{4}{\pi\hbar v_F} \sum_m |\psi(k_\varepsilon, r)|^2, \qquad k_\varepsilon = -\frac{\varepsilon}{\hbar v_F}, \quad (11)$$

where ψ is the two-component Dirac wave function (5) [18]. This quantity can be directly measured by scanning tunneling spectroscopy probes. Evaluating the sum over m in (11), we obtain LDOS map shown in Fig. 4.

Several quasibound states are seen in LDOS maps (Fig. 4) as local resonances at $\varepsilon < 0$. The values of β were chosen to illustrate that the width Γ of each resonance scales with ε, while its spatial extent scales as $1/\varepsilon$, in agreement with our quasiclassical analysis and Eq. (7).

A distinct advantage of local probes, as opposed to transport, is that the supercritical impurities do not need to be a majority. In fact, it suffices to locate just one nonunivalent impurity and perform STM imaging in vicinity. Alternatively, one can identify groups of two or three

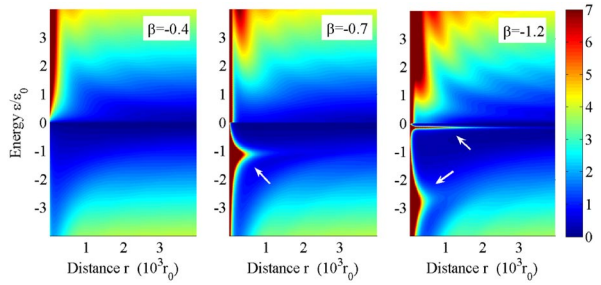

FIG. 4 (color online). Spatial map of the local density of states (LDOS) near a charge impurity, Eq. (11). The signatures of the quasibound states are resonances appearing at $\beta < -\frac{1}{2}$ at $r \sim 0$ and $\varepsilon < 0$ (marked by arrows). Note the localization length that scales inversely with ε, and the linewidth proportional to ε, as predicted by Eq. (7). The intensity of the resonances is well in excess of the asymptotic value $\nu(\varepsilon) \propto |\varepsilon|$ at large r. Periodic modulation at $\varepsilon > 0$ with maxima at $kr \approx \pi n$ is the standing wave oscillation [18] ($k = \varepsilon/\hbar v_F$, $\varepsilon_0 = 10^{-3}\hbar v_F/r_0$).

univalent impurities that act together as one supercritical impurity, or even deliberately create such a group by inducing local charge by voltage applied to STM tip.

To conclude, while massless particles cannot form discrete states, a family of quasibound states appears in the presence of a supercritical Coulomb potential. These states manifest themselves as resonances in transport coefficients and in the local density of states, providing a clear signature of the supercritical regime.

This work is supported by the DOE (Contract No. DEAC 02-98 CH 10886), FOM (The Netherlands), NSF-MRSEC (No. DMR 02132802) and NSF-NIRT No. DMR-0304019.

[1] A. K. Geim and K. S. Novoselov, Nat. Mater. **6**, 183 (2007).
[2] J. González, F. Guinea, and M. A. H. Vozmediano, Nucl. Phys. B **424**, 595 (1994).
[3] M. I. Katsnelson, K. S. Novoselov, and A. K. Geim, Nature Phys. **2**, 620 (2006).
[4] M. I. Katsnelson and K. S. Novoselov, Solid State Commun. **143**, 3 (2007).
[5] V. V. Cheianov, V. I. Fal'ko, and B. L. Altshuler, Science **315**, 1252 (2007).
[6] A. Rycerz, J. Tworzydlo, and C. W. J. Beenakker, Nature Phys. **3**, 172 (2007).
[7] D. A. Abanin and L. S. Levitov, Science **317**, 641 (2007).
[8] Y. B. Zeldovich and V. S. Popov, Usp. Fiz. Nauk **105**, 403 (1971) [Sov. Phys. Usp. **14**, 673 (1972)].
[9] W. Greiner, B. Muller, and J. Rafelski, *Quantum Electrodynamics of Strong Fields* (Springer-Verlag, Berlin, 1985).
[10] S. J. Brodsky, SLAC report 1337 (unpublished).
[11] C. G. Darwin, Philos. Mag. **25**, 201 (1913).
[12] I. Pomeranchuk and Y. Smorodinsky, J. Phys. (USSR) **9**, 97 (1945).
[13] K. Nomura and A. H. MacDonald, Phys. Rev. Lett. **96**, 256602 (2006).
[14] T. Ando, J. Phys. Soc. Jpn. **75**, 074716 (2006).
[15] E. H. Hwang, S. Adam, and S. Das Sarma, Phys. Rev. Lett. **98**, 186806 (2007).
[16] K. S. Novoselov *et al.* Nature (London) **438**, 197 (2005).
[17] P. M. Ostrovsky, I. V. Gornyi, and A. D. Mirlin, Phys. Rev. B **74**, 235443 (2006).
[18] A. Shytov, M. Katsnelson, and L. Levitov, Phys. Rev. Lett. **99**, 236801 (2007).
[19] V. M. Pereira, J. Nilsson, and A. H. Castro Neto, arXiv:0706.2872.
[20] R. R. Biswas, S. Sachdev, and D. T. Son, arXiv:0706.3907.
[21] M. Fogler, D. Novikov, and B. Shklovskii, arXiv:0707.1023.
[22] D. S. Novikov, arXiv:0706.1391.
[23] M. S. Dresselhaus and G. Dresselhaus, Adv. Phys. **51**, 1 (2002).
[24] T. E. Weller *et al.*, Nature Phys. **1**, 39 (2005).
[25] A. M. Shikin *et al.*, Phys. Rev. B **51**, 13586 (1995).
[26] T. Mori *et al.*, J. Phys. Soc. Jpn. **69**, 3051 (2000).
[27] J. L. McChesney *et al.*, arXiv:0705.3264.
[28] P. G. Silvestrov and K. B. Efetov, Phys. Rev. Lett. **98**, 016802 (2007).
[29] H.-Y. Chen, V. Apalkov, and T. Chakraborty, Phys. Rev. Lett. **98**, 186803 (2007).